Nonlinearity-Tuned Optical Spin-Orbit Interaction of Graphene-Wrapped Nanoparticles

Xiaoying Gu, Yuchen Sun, Lei Gao, Andrey Novitsky, Wenjing Yu, and Dongliang Gao

***Abstract*—Nonlinear control of light-matter interaction plays an important role in various optical phenomena, including spin-orbit interaction of light. In this paper, we demonstrate that the spin-orbit interaction of graphene-wrapped nanoparticles can be tuned by the input intensity of light. Typical optical bistable responses are observed in the scattering efficiency and the local electric fields. In the optical bistable regime, the strength of spin-orbit interaction in the near-field is significantly tuned in the switching-up and switching-down branches. The tunability of spin-orbit interaction enables promising nonlinear control schemes in nanophotonic devices.**

***Index Terms*—Graphene, nanoparticle, nonlinear, optical bistability, spin-orbit interaction.**

I. Introduction

ELECTROMAGNETIC fields can inherently have both spin angular momentum (SAM) and orbital angular momentum (OAM), which are independent of each other when the electromagnetic fields propagate in free space. The spin-orbit interaction (SOI), i.e., the transformation between SAM and OAM, occurs when the electromagnetic fields are focused, reflected, or scattered [1], [2]. SOI is one of the striking features in the research fields of light-matter interactions. Many interesting phenomena are associated with the SOI, such as the spin-momentum locking [3], [4], [5], and photonic Skyrmions [6], [7]. The SOI can find various applications in metamaterials and metasurfaces, such as giant photonic spin Hall effect [8], [9], [10], [11], [12], [13], [14], optical differential operations [15], [16], and all-optical image edge detection [17], [18], [19]. Among them, Luo et al. have done a series of interesting research works. For example, they have proposed the first unified description of spin Hall effect of light by the spin redirection and Pancharatnam-Berry phases, and directly observed giant photonic spin Hall effect in a dielectric-based metamaterial [11]. And then, with the spin-orbit interaction of light in the photonic Dirac metacrystal, they found a giant photonic spin Hall effect near the Dirac points in 2020 [14]. Meanwhile, they have reported a full optical differentiator at a simple optical interface, and the optical differential operation is independent of the wavelength [15]. In addition, Luo et al. have proposed a mechanism of edge detection based on a highly efficient dielectric metasurface and experimentally demonstrated broadband edge detection in 2019 [18]. Recently, He et al. have successfully further reduced the complexity of edge detection systems by integrating focusing and differentiation capabilities onto a monolithic metasurface through asymmetric photonic spin-orbit interactions [19]. Various methods have been developed to manipulate the spin-orbit coupling in nanophotonic devices. For example, induced singularity by interference is proposed to enhance the SOI of light in a uniaxial slab [20]. Nanostructures with graphene are widely used to tune and control SOI as well as spin Hall effect of light [21], [22]. Indeed, doping can confer various new or improved optical, electromagnetic, and structural properties on graphene, thus greatly extending the arsenal of graphene materials and their potential for a spectrum of applications. Different dopants, doping configurations and their relative ratios, and compositions of co-dopants give graphene distinct properties [23].

Recently, nonlinear control has attracted much attention in tuning parity-time symmetry [24], photonic topological insulator [25], and optical bound states in the continuum [26]. Nonlinear spin-orbit interaction of light can offer additional degree of freedom to engineer structured light [27], [28]. In the linear optical processes, the conversion of SAM to OAM is independent of the incident light intensity. In contrast, in the nonlinear optical processes, the SOI can be controlled by tuning the input intensity of light. Nonlinearity shows great potentials in the application of optical angular momentum [29], [30], [31]. What's more, high-order nonlinear SOI is demonstrated by plasmonic metasurfaces in nonlinear waves [32].

In this paper, we study the spin-orbit interaction of graphene-wrapped nanoparticles under the incidence of circularly polarized light. We develop the nonlinear quasistatic theory on graphene-wrapped nanosphere with right circularly polarized (RCP) light. Typical optical bistable responses are found in the

Manuscript received 28 July 2022; revised 8 October 2022; accepted 28 October 2022. Date of publication 2 November 2022; date of current version 10 November 2022. This work was supported in part by the National Natural Science Foundation of China under Grants 92050104 and 11904141, in part by Suzhou Prospective Application Research Project under Grant SYG202039, and in part by the Natural Science Foundation of Jiangsu Province under Grant BK20191031. *(Corresponding authors: Lei Gao; Wenjing Yu.)*

Xiaoying Gu, Yuchen Sun, and Dongliang Gao are with the School of Physical Science and Technology and Engineering Research Center of Digital Imaging and Display, Ministry of Education Soochow University, Suzhou 215006, China (e-mail: 20224208019@stu.suda.edu.cn; 1922401018@stu.suda.edu.cn; dlgao@suda.edu.cn).

Lei Gao is with the School of Physical Science and Technology and Engineering Research Center of Digital Imaging and Display, Ministry of Education Soochow University, Suzhou 215006, China, and also with the School of Optical and Electronic Information Suzhou City University, Suzhou 215104, China (e-mail: leigao@suda.edu.cn).

Andrey Novitsky is with the Department of Theoretical Physics and Astrophysics, Belarusian State University (BSU), Nezavisimosti Avenue 4 220030 Minsk, Belarus (e-mail: novitsky@bsu.by).

Wenjing Yu is with the School of Mathematics and Physics, Jiangsu University of Technology, Changzhou 213001, China (e-mail: yuwj@jsut.edu.cn).

Digital Object Identifier 10.1109/JPHOT.2022.3218815

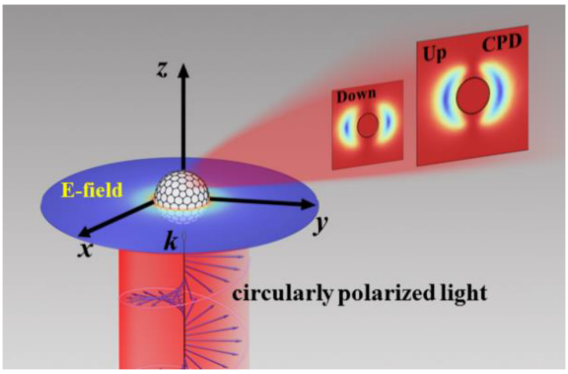

Fig. 1. Illustration of the graphene-wrapped nanoparticle under the incidence of circularly polarized light. The insets are the distributions of circular polarization degree (CPD) in the near field, which character the conversion between SAM and OAM for different input intensities of light.

far-field scattering and near-field intensity, which are verified by nonlinear full-wave simulation. Our results show that the SOI effect can be tuned by the input intensity in the optical bistable regime. The circular polarization degree (CPD) in the near field, which characters the conversion between SAM and OAM, demonstrates obvious different strengths for switching-up and switching-down input intensity of light. This tunability of SOI is realized by controlling the surface current density of graphene, whose nonlinear optical response occurs when the particle is in an intense incident light [33], [34], [35], [36]. Our work offers an alternative way to control the spin-orbit interaction of near-field [37].

II. Theoretical Models

Fig. 1 illustrates the considered graphene-wrapped nanoparticle with radius a and relative permittivity ε. For simplicity, we set the host medium as vacuum with relative permittivity ε_h. In this paper, the size of nanoparticle ($a = 50$ nm) that we studied is much smaller than the incident wavelength (above 10 μm). Hence the quasistatic approximation (QSA) can be adopted to obtain the local fields of the nanoparticles. The electric potentials satisfy the Laplace equation: $\nabla^2\phi_n = 0$, where the subscript $n = c$ stands for inside the particle and $n = h$ in the host medium. For the incidence of RCP light $E = (E_0/\sqrt{2})(\hat{\mathbf{e}}_x + i\hat{\mathbf{e}}_y)e^{ikz}e^{-i\omega t}$ [38], one can derive the general solutions of the above Laplace equation as,

$$\begin{aligned}\phi_c &= -A(E_0/\sqrt{2})r\cos\theta - iA(E_0/\sqrt{2})r\cos\theta' \\ \phi_h &= -(E_0/\sqrt{2})\left(r - Br^{-2}\right)\cos\theta - i(E_0/\sqrt{2})\left(r - Br^{-2}\right)\cos\theta'\end{aligned} \tag{1}$$

The graphene layer on the nanoparticle's surface is considered as a thin conducting shell, which contributes to the conductivity σ in the boundary conditions [39].

$$\begin{aligned}\hat{n}\times(\mathbf{E}_h - \mathbf{E}_c)|_{r=a} &= 0 \\ \hat{n}\cdot(\mathbf{D}_h - \mathbf{D}_c)|_{r=a} &= \frac{1}{i\omega}\nabla_s\cdot\mathbf{J}\end{aligned} \tag{2}$$

where $\mathbf{J} = \sigma\mathbf{E} \approx \sigma\mathbf{E}_c$ represents the surface current density. Here, the operator ∇_s stands for surface divergence, and $\mathbf{E}_c$ is the linear local electric field inside the nanoparticle.

Solving (1) and (2), one can obtain the unknown coefficients A and B,

$$A = \frac{3\varepsilon_h}{\varepsilon + 2\varepsilon_h + 2\Theta},\ B = \frac{\varepsilon - \varepsilon_h + 2\Theta}{\varepsilon + 2\varepsilon_h + 2\Theta}a^3 \tag{3}$$

where $\Theta = i\sigma/(\omega a\varepsilon_0)$ and B is the dipole polarizability of the graphene-wrapped sphere.

In this paper, the nonlinear surface conductivity of graphene are simplified and described by the random-phase approximation [40], [41]

$$\tilde{\sigma}_g = \sigma_g + \sigma_3|\mathbf{E}_c|^2 \tag{4}$$

where the simplified linear term σ_g and the Kerr nonlinear surface conductivity σ_3 are shown as follows [40], [42]

$$\sigma_g = \frac{ie^2E_F}{\pi\hbar^2(\omega + i/\tau)},\ \sigma_3 = -i\frac{9e^4\upsilon_F^2}{8\pi E_F\hbar^2\omega^3} \tag{5}$$

where e, E_F, $\hbar$, υ_F, and τ are the electron charge, Fermi energy, reduced Planck constant, Fermi velocity of electrons, and the electron-phonon relaxation time, respectively.

According to quasistatic approximation, the local electric field E_c inside the nanoparticle and the external field E_0 are related by

$$E_c = \frac{3\varepsilon_h}{\varepsilon + 2\varepsilon_h + 2i\tilde{\sigma}_g/(\omega a\varepsilon_0)}E_0 \tag{6}$$

Equation (6) is a nonlinear equation since it contains the nonlinear surface conductivity $\tilde{\sigma}_g$. Hence the optical bistable responses can be achieved. In addition, we calculate the normalized scattering efficiency Q_{sca} of the graphene-wrapped nanoparticle in the far field,

$$Q_{sca} = \mathrm{Re}\left[\frac{6}{k^2a^2}\left(-\frac{2i}{3}k^3\alpha\right)^2\right] \tag{7}$$

where $k = 2\pi\sqrt{\varepsilon_h}/\lambda_0$ is the wave number, and α is the electric polarizability including the radiation correction with the approximate static polarizability of the graphene-wrapped nanoparticle α_0 [43]

$$\alpha = \alpha_0\Big/\left(1 - i\frac{2}{3}\frac{k^3\alpha_0}{\varepsilon_h}\right),\ \alpha_0 = \frac{\varepsilon - \varepsilon_h + 2\Theta}{\varepsilon + 2\varepsilon_h + 2\Theta}\varepsilon_h a^3 \tag{8}$$

To verify the above theoretical analysis, we also performed the numerical simulation of this geometry with the finite element method (FEM) by COMSOL Multiphysics.

III. Results

Fig. 2(a) shows the normalized scattering efficiency Q_{sca} versus the incident wavelength λ. The continuous curves correspond to solutions obtained by the QSA. Specifically, the black line is the result when only linear term σ_g in (4) is considered, while the red and green curves are plotted considering the nonlinear surface conductivity $\tilde{\sigma}_g$ for various values of the incident electric field: $E_0 = 0.5$Mev(red line), and $E_0 = 1.5$Mev(green line).

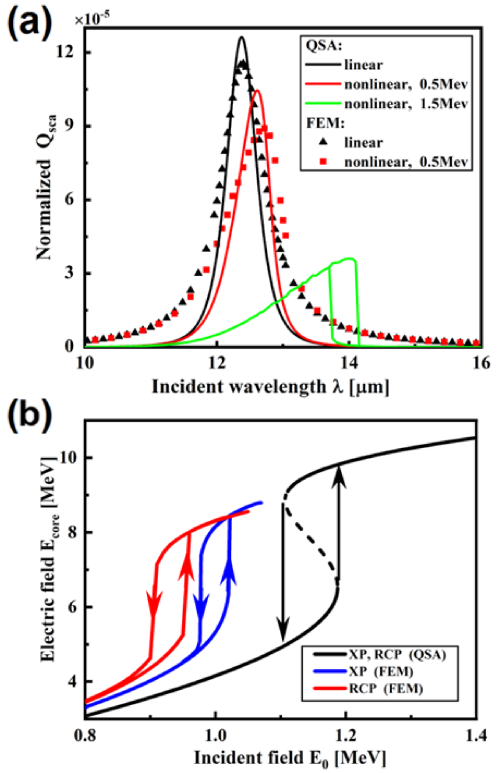

Fig. 2. (a) Normalized scattering efficiency spectra in both linear and nonlinear regimes obtained by the QSA and FEM respectively for right circularly polarized (RCP) incidence. (b) The electric field inside the nanoparticle as a function of the incident field for incident x-polarized (XP) and RCP waves. The nanoparticle's radius $a = 50$ nm, relative permittivity $\varepsilon = 2.25$ and the incident wavelength is 13.5 μm.

The resonant peak in scattering efficiency curves is due to the "metallic" graphene layer in the terahertz frequencies [44].

It clearly indicates that graphene's analogous Kerr nonlinearity on conductivity will generally result in a redshift of the resonant peak and decreased strength of the resonance. This is due to the fact that when the incident light's intensity increases, the eigen wavelengths will redshift for the Kerr-type metallic nonlinearity [45]. Compared the results obtained by the FEM with those of the QSA, the results are quite similar but with a minor difference. It is due to the theoretical approximations of the quasistatic limit, which is not applied in FEM. In the FEM, when we calculate the surface current density and nonlinear surface conductivity of graphene, we use the local electric field on the graphene's surface, instead of the electric field inside the nanoparticle, i.e., $\mathbf{J} = \sigma \mathbf{E}_{local}$ and $\tilde{\sigma}_g = \sigma_g + \sigma_3 |\mathbf{E}_{local}|^2$. Interestingly, when the optical field is relatively high ($E_0 = 1.5$Mev), optical bistable responses are observed, with two stable branches and an abrupt switching effect at the design wavelength.

Fig. 2(b) shows the optical bistable responses of E_c and the incident field E_0 for both XP and RCP light within the QSA and FEM, respectively. In the appropriate range of driving electric field, bistable responses are indeed found. As can be seen that when the incident field increases from a relatively low value (i.e., $E_0 = 0.8$Mev), the electric field E_c within the nanoparticle

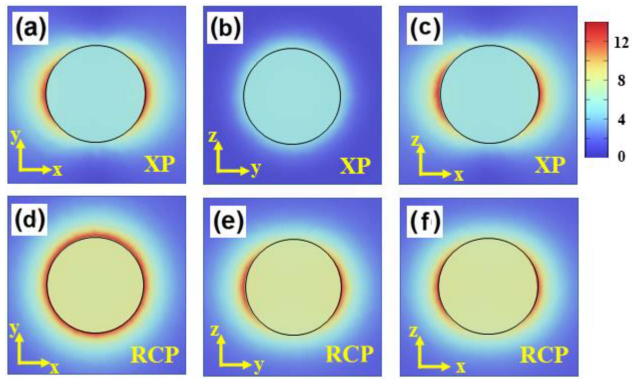

Fig. 3. (a)–(c) Distribution of the local electric fields in the x-y, y-z and x-z planes for the XP incidence, while (d)–(f) are for the RCP incidence. All the maps are calculated by FEM and share the same color bar.

first increases, and then jumps to the upper stable branch at the switching-up threshold field $E_{0,up}$. After that, the electric field E_c will monotonically increase with the incident field. Conversely, when the incident field decreases from a relatively high value (i.e., $E_0 = 1.4$Mev), E_c will discontinuously jump to the lower stable branch at the switching-down threshold field $E_{0,down}$. It should be noted that the dashed line in the plot represents the calculated unstable branch which is a mathematical solution of the nonlinear problem, but it is not reachable in practice. The effects of the nanoparticle parameters, such as particle size and relative permittivity, are consistent with previous work [46], [47], with details as follows. A larger particle size or larger ε, will generally result in a lower switching threshold field accompanied by a narrower bistable region.

From Fig. 2(b), one observes that the relationships between the internal E_c and incident electric fields E_0 are identical for the incidence of linear x-polarized light (XP with the form $E = E_0 \hat{\mathbf{e}}_x e^{ikz} e^{-i\omega t}$) and circularly polarized light in the case of the QSA. This is because the polarizability of the graphene-wrapped nanoparticle is independent of the incident polarization in the quasistatic limit. In the case of the FEM, however, the results are significantly distinguished. More importantly, for both polarized waves, the threshold fields calculated based on the FEM are all smaller than the result within the QSA. We reasonably speculate that this is because the QSA only considers the inner field E_c, but in fact the electric fields at the boundary are effectively enhanced which have been ignored in the calculation, as shown in Fig. 3. As expected, RCP waves require a smaller threshold field than XP waves, since they excite a stronger localized field and larger enhanced region in the surface of graphene (see the x-y plane of XP and RCP in Fig. 3(a) and (d)).

Bistability not only affects the far-field scattering efficiency described above, but also affects the near-field, such as spin-orbit interaction, as is shown in Fig. 4. The inserts in the plot are the distributions of circular polarization degree (CPD) for the near-field of different positions (marked as I, II, III, and IV) in two stable branches. Among them, positions II and IV share the same strength of incident field (0.93Mev). Here, we define CPD as $|\varepsilon_0 \mathbf{E}^* \times \mathbf{E} + \mu_0 \mathbf{H}^* \times \mathbf{H}| / (\varepsilon_0 |\mathbf{E}_0|^2 + \mu_0 |\mathbf{H}|^2)$, fulfilling CPD $= 1$ for the circular polarization [48].

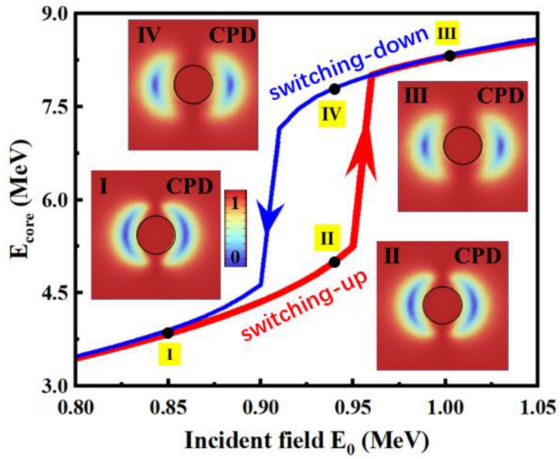

Fig. 4. Dependence of the electric field in the core on the external incident field E_0 for RCP incidence within FEM. The inserts (I to IV) are the distributions of CPD for the near-field of different positions, and they share the same color bar with a normalized color range.

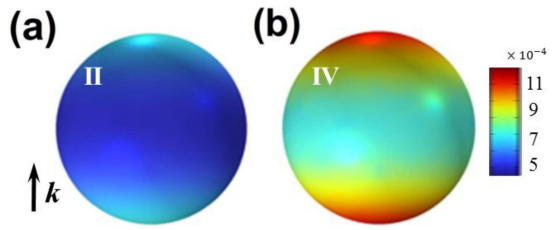

Fig. 5. Magnitude of the surface current density **J** on the graphene surface for (a) switching-up branch and (b) switching-down branch in the bistable region. The II and IV are corresponding to the same strength of the incident field in Fig. 4.

According to the characteristics of the bistable response, I→II→III and III→IV→I are through switching-up and switching-down branches, respectively. First, we focus on the process of increasing the incident field gradually. Remarkably, since both points I and II are in the lower stable branch, they yielded almost identical results. Meanwhile, the CPD drops to high values for the field in position III after the abrupt discontinuous jump at the threshold field $E_{0,up}$. The high CPD of the field in position III, as compared to the field in position II, implies that most of the OAM of the photons is converted to the SAM by means of the SOI in this region. Similarly, when the applied field is continuously decreased, the CPD first remains the same (III-IV) and then drops to low values for the field in position I after the abrupt discontinuous jump at the threshold field $E_{0,down}$. Conversely, the low CPD of the field in position I, as compared to the field in position IV, implies that most of the SAM of the photons is converted to the OAM by means of the SOI. Interestingly, the distributions of CPD in positions II and IV are quite different, although they have the same incident field intensity. This stems from the fact that the distributions and intensity of surface current density **J** on the surface of graphene, are completely different at these two points, as shown in Fig. 5. Since the boundary condition in (2) contains the surface current density **J**, when the surface current changes, the boundary condition will change accordingly. The Ohm's law $\mathbf{J} = \sigma\mathbf{E}$ connects the surface current density and the field distribution around the nanoparticles. Hence, the CPD difference can be related to the difference of graphene surface current.

IV. Conclusion

In conclusion, we have performed the theoretical investigations on graphene-wrapped nanosphere. We develop the nonlinear quasistatic theory with RCP incidence. As expected, typical optical bistable responses are found in the far-field scattering and near-field intensity. For comparison, we also performed a nonlinear full-wave simulation and good agreement is found. Furthermore, we study the SOI of graphene-wrapped nanoparticles under the incidence of RCP light. Our results show that the SOI effect can be tuned by the input intensity in the optical bistable regime. The CPD in the near field, which characters the conversion between SAM and OAM, demonstrates obvious different strengths for switching-up and switching-down input intensity of light. Intrinsically, this tunability of SOI is realized by controlling the surface current density of the monolayer graphene.

References

[1] O. G. Rodriguez-Herrera, D. Lara, K. Y. Bliokh, E. A. Ostrovskaya, and C. Dainty, "Optical nanoprobing via spin-orbit interaction of light," *Phys. Rev. Lett.*, vol. 104, no. 25, Jun. 2010, Art. no. 253601.

[2] K. Y. Bliokh, E. A. Ostrovskaya, M. A. Alonso, O. G. Rodriguez-Herrera, D. Lara, and C. Dainty, "Spin-to-orbital angular momentum conversion in focusing, scattering, and imaging systems," *Opt. Exp.*, vol. 19, no. 27, pp. 26132–26149, Dec. 2011.

[3] J. Petersen, J. Volz, and A. Rauschenbeutel, "Chiral nanophotonic waveguide interface based on spin-orbit interaction of light," *Science*, vol. 346, no. 6205, pp. 67–71, Oct. 2014.

[4] C. Triolo, A. Cacciola, S. Patanè, R. Saija, S. Savasta, and F. Nori, "Spin-momentum locking in the near field of metal nanoparticles," *ACS Photon.*, vol. 4, no. 9, pp. 2242–2249, Apr. 2017.

[5] M. S. Wang et al., "Spin-orbit-locked hyperbolic polariton vortices carrying reconfigurable topological charges," *eLight*, vol. 2, 2022, Art. no. 12.

[6] L. P. Du, A. P. Yang, A. V. Zayats, and X. C. Yuan, "Deep-subwavelength features of photonic skyrmions in a confined electromagnetic field with orbital angular momentum," *Nature Phys.*, vol. 15, no. 7, pp. 650–654, Jul. 2019.

[7] P. Shi, L. P. Du, M. J. Li, and X. C. Yuan, "Symmetry-protected photonic chiral spin textures by spin–orbit coupling," *Laser Photon. Rev.*, vol. 15, no. 9, Jul. 2021, Art. no. 2000554.

[8] D. L. Gao, R. Shi, A. E. Miroshnichenko, and L. Gao, "Enhanced spin Hall effect of light in spheres with dual symmetry," *Laser Photon. Rev.*, vol. 12, no. 11, Nov. 2018.

[9] D. Haefner, S. Sukhov, and A. Dogariu, "Spin Hall effect of light in spherical geometry," *Phys. Rev. Lett.*, vol. 102, no. 12, Mar. 2009, Art. no. 123903.

[10] X. B. Yin, Z. L. Ye, J. Rho, Y. Wang, and X. Zhang, "Photonic spin Hall effect at metasurfaces," *Science*, vol. 339, no. 6126, pp. 1405–1407, Mar. 2013.

[11] X. Ling et al., "Giant photonic spin Hall effect in momentum space in a structured metamaterial with spatially varying birefringence," *Light: Sci. Appl.*, vol. 4, no. 5, 2015, Art. no. e290.

[12] M. Liu, L. Cai, S. Chen, Y. Liu, H. Luo, and S. Wen, "Strong spin-orbit interaction of light on the surface of atomically thin crystals," *Phys. Rev. A*, vol. 95, no. 6, Jun. 2017, Art. no. 063827.

[13] Y.-H. Wang et al., "Photonic spin Hall effect by the spin-orbit interaction in a metasurface with elliptical nano-structures," *Appl. Phys. Lett.*, vol. 110, no. 10, 2017, Art. no. 101908.

[14] W. Xu et al., "Giant photonic spin Hall effect near the Dirac points," *Phys. Rev. A*, vol. 101, no. 2, Feb. 2020, Art. no. 023826.

[15] S. He, J. Zhou, S. Chen, W. Shu, H. Luo, and S. Wen, "Wavelength-independent optical fully differential operation based on the spin–orbit interaction of light," *APL Photon.*, vol. 5, no. 3, 2020, Art. no. 036105.

[16] W. Xu, X. Ling, D. Xu, S. Chen, S. Wen, and H. Luo, "Enhanced optical spatial differential operations via strong spin-orbit interactions in an anisotropic epsilon-near-zero slab," *Phys. Rev. A*, vol. 104, no. 5, Nov. 2021, Art. no. 053513.
[17] S. He, J. Zhou, S. Chen, W. Shu, H. Luo, and S. Wen, "Spatial differential operation and edge detection based on the geometric spin Hall effect of light," *Opt. Lett.*, vol. 45, no. 4, pp. 877–880, Feb. 2020.
[18] J. Zhou et al., "Optical edge detection based on high-efficiency dielectric metasurface," *Proc. Nat. Acad. Sci.*, vol. 116, no. 23, pp. 11137–11140, Jun. 2019.
[19] Q. He et al., "Monolithic metasurface spatial differentiator enabled by asymmetric photonic spin-orbit interactions," *Nanophotonics*, vol. 10, no. 1, pp. 741–748, 2020.
[20] Z. H. Chen, S. Lin, J. H. Hong, L. J. Sheng, Y. Chen, and X. X. Zhou, "Enhanced photonic spin Hall effect via singularity induced by destructive interference," *Opt. Lett.*, vol. 46, no. 19, pp. 4883–4886, Oct. 2021.
[21] Z. Y. Zhang et al., "Spin-orbit coupling in photonic graphene," *Optica*, vol. 7, no. 5, pp. 455–462, Jun. 2020.
[22] M. Cheng et al., "Tunable and enhanced spin Hall effect of light in layered nanostructures containing graphene," *J. Opt. Soc. Amer. B*, vol. 35, no. 8, pp. 1829–1835, Aug. 2018.
[23] X. Wang, G. Sun, P. Routh, D. H. Kim, W. Huang, and P. Chen, "Heteroatom-doped graphene materials: Syntheses, properties and applications," *Chem. Soc. Rev.*, vol. 43, no. 20, pp. 7067–7098, 2014.
[24] S. Q. Xia et al., "Nonlinear tuning of PT symmetry and non-Hermitian topological states," *Science*, vol. 372, no. 6537, pp. 72–76, Apr. 2021.
[25] L. J. Maczewsky et al., "Nonlinearity-induced photonic topological insulator," *Science*, vol. 370, no. 6517, pp. 701–704, Nov. 2020.
[26] K. Koshelev et al., "Subwavelength dielectric resonators for nonlinear nanophotonics," *Science*, vol. 367, no. 6475, pp. 288–292, Jan. 2020.
[27] Y. T. Tang, K. F. Li, X. C. Zhang, J. H. Deng, G. X. Li, and E. Brasselet, "Harmonic spin–orbit angular momentum cascade in nonlinear optical crystals," *Nature Photon.*, vol. 14, no. 11, pp. 658–662, Nov. 2020.
[28] F. X. Guan et al., "Spin-orbit interactions in a nonlinear medium due to a nonlinear-induced geometric phase," *Opt. Lett.*, vol. 46, no. 11, pp. 2758–2761, Jun. 2021.
[29] M. Y. Su et al., "Identification of optical orbital angular momentum modes with the Kerr nonlinearity of few-layer WS_2," *2D Mater.*, vol. 7, no. 2, Jan. 2020, Art. no. 025012.
[30] Z. G. Chen and M. Segev, "Highlighting photonics: Looking into the next decade," *eLight*, vol. 1, no. 1, Jun. 2021, Art. no. 2.
[31] P. F. Qi et al., "Phonon scattering and exciton localization: Molding exciton flux in two dimensional disorder energy landscape," *eLight*, vol. 1, no. 1, Nov. 2021, Art. no. 6.
[32] S. Chen, K. Li, J. Deng, G. Li, and S. Zhang, "High-order nonlinear spin-orbit interaction on plasmonic metasurfaces," *Nano Lett.*, vol. 20, no. 12, pp. 8549–8555, Jun. 2020.
[33] Y. Guo et al., "Gas detection in a graphene based dual-mode fiber laser microcavity," *Sensors Actuators B: Chem.*, vol. 348, 2021, Art. no. 130694.
[34] W. Chen, Y. Wang, and W. Ji, "Two-photon absorption in graphene enhanced by the excitonic Fano resonance," *J. Phys. Chem. C*, vol. 119, no. 29, pp. 16954–16961, Jul. 2015.
[35] Y. Li et al., "Nonlinear co-generation of graphene plasmons for opto-electronic logic operations," *Nature Commun.*, vol. 13, no. 1, Jun. 2022, Art. no. 3138.
[36] N. An et al., "Electrically tunable four-wave-mixing in graphene heterogeneous fiber for individual gas molecule detection," *Nano Lett.*, vol. 20, no. 9, pp. 6473–6480, Sep. 2020.
[37] K. Zhao, X. Z. Xu, W. Ren, D. Y. Jin, and P. Xi, "Two-photon MINFLUX with doubled localization precision," *eLight*, vol. 2, no. 1, 2022, Art. no. 5.
[38] F. Pineider et al., "Circular magnetoplasmonic modes in gold nanoparticles," *Nano Lett.*, vol. 13, no. 10, pp. 4785–4789, Sep. 2013.
[39] D. A. Smirnova, I. V. Shadrivov, A. E. Miroshnichenko, A. I. Smirnov, and Y. S. Kivshar, "Second-harmonic generation by a graphene nanoparticle," *Phys. Rev. B*, vol. 90, no. 3, Jul. 2014, Art. no. 035412.
[40] N. M. R. Peres, Y. V. Bludov, J. E. Santos, A.-P. Jauho, and M. I. Vasilevskiy, "Optical bistability of graphene in the terahertz range," *Phys. Rev. B*, vol. 90, no. 12, Sep. 2014, Art. no. 125425.
[41] R. J. Li, X. Lin, S. S. Lin, X. M. Zhang, E. Li, and H. S. Chen, "Graphene induced mode bifurcation at low input power," *Carbon*, vol. 98, pp. 463–467, Mar. 2016.
[42] T. Christensen, W. Yan, A.-P. Jauho, M. Wubs, and N. A. Mortensen, "Kerr nonlinearity and plasmonic bistability in graphene nanoribbons," *Phys. Rev. B*, vol. 92, no. 12, Sep. 2015, Art. no. 121407.
[43] D. L. Gao, R. Shi, Y. Huang, and L. Gao, "Fano-enhanced pulling and pushing optical force on active plasmonic nanoparticles," *Phys. Rev. A*, vol. 96, no. 4, Oct. 2017, Art. no. 043826.
[44] A. Vakil and N. Engheta, "Transformation optics using graphene," *Science*, vol. 332, no. 6035, pp. 1291–1294, Jul. 2011.
[45] W. J. Yu, P. J. Ma, H. Sun, L. Gao, and R. E. Noskov, "Optical tristability and ultrafast Fano switching in nonlinear magnetoplasmonic nanoparticles," *Phys. Rev. B*, vol. 97, no. 7, Feb. 2018, Art. no. 075436.
[46] K. Zhang, Y. Huang, A. E. Miroshnichenko, and L. Gao, "Tunable optical bistability and tristability in nonlinear graphene-wrapped nanospheres," *J. Phys. Chem. C*, vol. 121, no. 21, pp. 11804–11810, May 2017.
[47] Y. Huang, A. E. Miroshnichenko, and L. Gao, "Low-threshold optical bistability of graphene-wrapped dielectric composite," *Sci. Rep.*, vol. 6, Mar. 2016, Art. no. 23354.
[48] D. Pan, H. Wei, L. Gao, and H. X. Xu, "Strong spin-orbit interaction of light in plasmonic nanostructures and nanocircuits," *Phys. Rev. Lett.*, vol. 117, no. 16, Oct. 2016, Art. no. 166803.